PHYSICAL REVIEW MATERIALS **1**, 044404 (2017)

Electronic structure and magnetism in the layered triangular lattice compound $CeAuAl_4Ge_2$

S. Zhang,[1,2] N. Aryal,[1,2] K. Huang,[1] K.-W. Chen,[1,2] Y. Lai,[1,2] D. Graf,[1] T. Besara,[1]
T. Siegrist,[1,3] E. Manousakis,[1,2,4] and R. E. Baumbach[1,2,*]

[1]*National High Magnetic Field Laboratory, Florida State University, Tallahassee, Florida 32306, USA*
[2]*Department of Physics, Florida State University, Tallahassee, Florida 32306, USA*
[3]*Department of Chemical and Biomedical Engineering, FAMU-FSU College of Engineering, Tallahassee, Florida 32310, USA*
[4]*Department of Physics, National and Kapodistrian University of Athens, Athens 15784, Greece*

(Received 19 May 2017; published 25 September 2017)

Results are reported for the f-electron intermetallic $CeAuAl_4Ge_2$, where the atomic arrangement of the cerium ions creates the conditions for possible geometric frustration. The magnetic susceptibility follows a Curie-Weiss temperature dependence at elevated temperatures, revealing that the cerium ions are trivalent. At lower temperatures the crystal electric field splits the Hund's rule multiplet, resulting in a weak low-temperature magnetic exchange interaction and ordering near $T_M \approx 1.4$ K. This occurs within a metallic Kondo lattice, where electrical resistivity and heat capacity measurements show that the Kondo-driven electronic correlations are negligible. Quantum oscillations are detected in ac-magnetic susceptibility measurements and uncover small charge carrier effective masses. Electronic structure calculations reveal that inclusion of an on-f-site Coulomb repulsion (Hubbard) U results in antiferromagnetic order and causes the f-electron bands to move away from the Fermi level, resulting in electronic behavior that is dominated by the s, p, and d bands, which are all characterized by light electron masses. Thus, $CeAuAl_4Ge_2$ may provide a starting point for investigating geometric magnetic frustration in a cerium lattice without strong Kondo hybridization, where calculations provide useful guidance.

DOI: 10.1103/PhysRevMaterials.1.044404

I. INTRODUCTION

An attractive feature of correlated electron metals is that they often host multiple nearly degenerate electronic ground states, including charge order, spin order, multipolar order, superconductivity, heavy fermion behavior, breakdown of the Fermi liquid, and other intriguing phenomena [1–4]. For materials containing f-electron elements with unstable valences (e.g., Ce and Yb), the behavior is associated with the competition between Kondo hybridization and RKKY interactions [5,6]. However, rich behavior can also be driven by magnetic frustration, which promotes complex ordering and might even lead to a quantum spin liquid state under some circumstances [7–10]. While this is an intriguing possibility, there is currently a lack of model systems to study, particularly for metals. Clearly, then, it is desirable to uncover new f-electron metals with conditions for magnetic frustration.

Examples of f-electron materials with complex magnetism include $YbRh_2Si_2$ [11], $CeRhIn_5$ [12], YbAgGe [13], CePdAl [14], and CeRhSn [15]. In tetragonal $YbRh_2Si_2$ and $CeRhIn_5$ the magnetic complexity presumably arises from fine balancing of the nearest neighbor, next nearest neighbor, etc. RKKY-mediated interactions, which might be described in terms of a picture like the anisotropic next-nearest-neighbor Ising (ANNNI) model [16]. In YbAgGe and CePdAl, magnetic frustration arises from the geometric arrangement of the f-electron ions in the crystalline lattice. Despite the differing origins of their magnetic behavior, these compounds are connected by the presence of strong hybridization between the f-electron and the conduction-electron states through the Kondo interaction. While this is often desirable, since strong hybridization can promote novel behavior, it also complicates the task of isolating which phenomena are primarily associated with magnetism. Thus it is important to find model systems where the hybridization strength is weak. Work on compounds such as LnT_2X_2M (Ln = lanthanide, T = Fe, Ru, Os, X = Al, Ga, and M = C, B [17,18], where ANNNI-type magnetic frustration may shape the ordered ground state, has made some progress in this direction, but it would be instructive to investigate other weakly correlated f-electron materials with the simpler condition of being geometrically frustrated.

Here we present results for single-crystalline $CeAuAl_4Ge_2$, which forms in a layered rhombohedral structure with well-separated planes of trivalent cerium ions that are distributed on a triangular lattice, which, in some situations, can result in geometric frustration [19]. The high-temperature magnetic susceptibility is anisotropic, with an antiferromagnetic exchange interaction along the c axis and a ferromagnetic in-plane exchange interaction that would not result in magnetic frustration. Crystal electric-field splitting of the Hund's rule multiplet modifies the low-temperature magnetism and results in small but negative Curie-Weiss temperatures for both directions, possibly setting the stage for weak geometric magnetic frustration. From specific heat and electrical resistivity measurements, we find magnetic order near $T_M \approx 1.4$ K. Interestingly, we also observe some evidence of magnetic fluctuations developing near 15 K. Thermodynamic, electrical transport, and quantum oscillation measurements reveal that the Kondo hybridization strength is weak, resulting in simple metallic behavior. Electronic structure calculations further reveal that by including the on-f-site Coulomb repulsion (Hubbard) U antiferromagnetic order emerges and the f-electron bands move away from the Fermi level. This results in electronic behavior that is dominated by the s, p, and d bands, which are all characterized by light electron masses. The calculated

*baumbach@magnet.fsu.edu

Fermi surface and associated quasiparticle effective masses are straightforward to understand in terms of quantum oscillations that are seen in ac-magnetic susceptibility measurements. With these results, we show that $CeAuAl_4Ge_2$ may be a useful starting point from which to uncover phenomena resulting from geometric magnetic frustration in a weakly correlated f-electron metal, where calculations provide quantitative guidance.

II. EXPERIMENTAL DETAILS

Single crystals of $CeAuAl_4Ge_2$ were grown using elements with purities >99.9% in a molten Al flux. The starting elements were loaded into a 2-mL alumina crucible at the ratio 1(Ce):1(Au):10(Al):5(Ge). The crucible was sealed under vacuum in a quartz tube, heated up to 1000 °C at a rate of 83 °C/h, kept at 1000 °C for 15 h, then cooled to 860 °C at a rate of 7 °C/h and held at 860 °C for 48 h, followed by cooling down to 700 °C at a rate of 12 °C/h. After removing the excess flux by centrifuging the tubes, single-crystal platelets with typical dimensions of several millimeters in width and height and 0.5- to 1-mm thickness were collected. The crystals form as trigonal plates, and single-crystal x-ray diffraction shows that the c axis is perpendicular to the hexagonal plane.

Sample composition and structure characterization were performed by single-crystal x-ray diffraction at room temperature using an Oxford Diffraction Xcalibur2 CCD system with graphite monochromated Mo$K\alpha$ radiation. Data were collected using ω scans with 1° frame widths to a resolution of 0.5 Å, equivalent to $2\theta = 90°$. Data collection, indexation, and absorption correction were performed using the Rigaku Oxford Diffraction CrysAlisPro software [20]. Subsequent structure refinement was carried out using CRYSTALS [21], employing Superflip [22], with starting parameters from the literature [23,24] to refine the structure. The data quality allowed for a full matrix refinement against F^2, with anisotropic thermal displacement parameters of all atoms in the structure. The occupancies of all atoms were relaxed but deviated negligibly from full occupancy. A crystallographic information file has been deposited with ICSD (CSD No. 431206) [25].

Magnetization $M(H,T)$ measurements were performed on a single crystal at temperatures $T = 1.8$–300 K under an applied magnetic field of $H = 0.5$ T and for $0 < H < 7$ T at a temperature $T = 1.8$ K for H applied both parallel ($\parallel$) and perpendicular ($\perp$) to the c axis using a Quantum Design VSM Magnetic Property Measurement System. The specific heat $C(T)$ was measured for $T = 0.5$–20 K and the electrical resistivity $\rho(T)$ was measured for $T = 0.6$–300 K using a Quantum Design Physical Property Measurement System. The ac susceptibility measurements were performed on a $CeAuAl_4Ge_2$ single crystal using a superconducting magnet at the National High Magnetic Field Laboratory under a sweeping field of $H = 0$–18 T for several temperatures T and also for several angles θ, where $\theta = 0$ is defined as $H \parallel c$.

Electronic structure calculations were performed using the WIEN2k package in the full-potential linearized augmented plane-wave and localized orbital basis framework [26] within the PBE parametrization of the generalized gradient approximation [27]. The plane-wave cutoff parameter $R_{MT}K_{max}$ was chosen to be 7, where R_{MT} is the muffin-tin radius and K_{max} is the maximum size of the reciprocal lattice vectors.

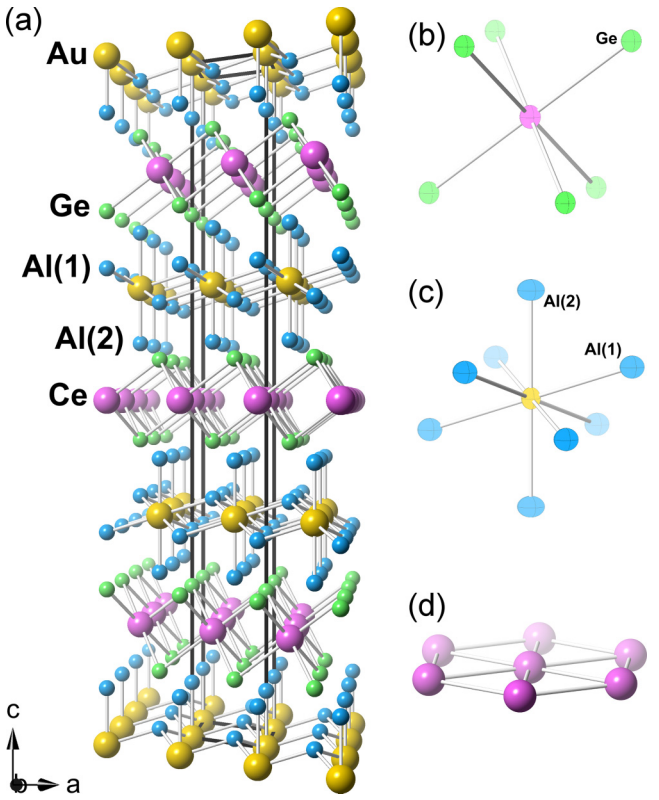

FIG. 1. (a) Crystal structure of $CeAuAl_4Ge_2$. (b, c) Local environment of Ce and Au displaying anisotropic displacement ellipsoids with 95% probability at 295 K. (d) Ce plane showing the equilateral triangle arrangement.

III. RESULTS

$CeAuAl_4Ge_2$ crystallizes in the rhombohedral space group $R\bar{3}m$ (No. 166) with unit cell parameters $a = 4.2334(2)$ Å and $c = 31.568(1)$ Å. This structure [Fig. 1(a)]—explored in more detail by Wu and Kanatzidis [23]—can be described as alternating layers of Ce and Au, stacked in an ...ABCABC... sequence. The Ce is octahedrally coordinated by Ge [Fig. 1(b)], while Au is surrounded by Al, forming a distorted cubic local environment [Fig. 1(c)]. Both the Ce-centered octahedra and the Au-centered cubes are edge sharing. Focusing on the Ce layers, the Ce atoms form a network of equilateral triangles in the ab plane separated by the lattice constant a [Fig. 1(d)] and with the planes 1/3 of the c-axis lattice constant apart ($d_{interplane} \approx 10.5$ Å), in essence creating a two-dimensional f-electron system where the triangular arrangement satisfies one condition for geometric frustration. Measurements of the crystals reported here show that the atomic site occupancy factors deviated negligibly from full occupancy, indicating a stoichiometric, high-quality crystal. Further details of the x-ray diffraction refinement and the structure are listed in Table I.

The magnetic susceptibility data $\chi(T) = M(T)/H$ for $CeAuAl_4Ge_2$ in $H = 0.5$ T applied parallel and perpendicular to the c axis are presented in Fig. 2. The data follow a Curie-Weiss temperature dependence at 150 K $\leqslant T \leqslant$ 300 K

TABLE I. Top: Crystallographic data and single-crystal x-ray diffraction collection and refinement parameters, obtained at ambient temperature. Bottom: Atomic coordinates and equivalent thermal displacement parameters (in $\times 10^4$ Å^2).

Compound					$CeAuAl_4Ge_2$	
Formula weight (g/mol)					590.20	
Space group					$R\bar{3}m$ (No. 166)	
a (Å)					4.2334(2)	
c (Å)					31.568(1)	
ρ_{calc} (g/cm^3)					6.000	
Z					3	
Atom	Site	Occupancy	x	y	z	U_{eq}
Ce	3b	1	0	0	0.5	87(5)
Au	3a	1	0	0	0	74(3)
Al(1)	6c	1	0	0	0.30849(9)	104(7)
Al(2)	6c	1	0	0	0.08206(8)	119(5)
Ge	6c	1	0	0	0.22528(2)	80(3)

[Fig. 2(b)], given by the expression

$$\chi = \frac{C}{(T-\theta)}, \tag{1}$$

where fits to the data yield $\theta = -90$ K for $H \parallel c$ (24 K for $H \perp c$) and $C = 0.73$ cm^3 K/mol (0.79 cm^3 K/mol), giving effective magnetic moments $\mu_{eff} \approx 2.42\mu_B$/Ce (2.51 μ_B/Ce), close to the expected Hund's rule value ($\mu_{eff} = 2.54\mu_B$/Ce). The anisotropy between the $H \parallel c$ and the $H \perp c$ curves reveals that the ab plane is the easy axis for magnetization and that antiferromagnetic and ferromagnetic exchange interactions occur in the $H \parallel c$ and $H \perp c$ directions, respectively. These trends are emphasized in Fig. 2(c), where (i) χT approaches 0.8 cm^2 K/mol at 300 K, as expected for trivalent Ce, and (ii) the χT curves for $H \parallel c$ and $H \perp c$ axis decrease and increase with decreasing T, consistent with antiferromagnetic and ferromagnetic exchange interactions,

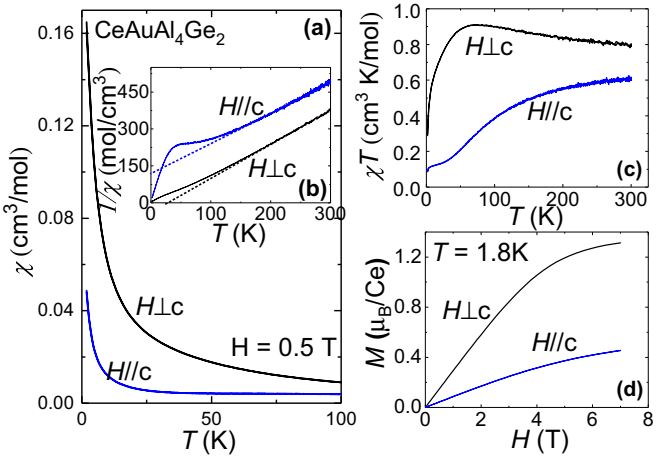

FIG. 2. (a) Magnetic susceptibility $\chi(T) = M(T)/H$ for $H = 0.5$ T applied parallel and perpendicular to the c axis vs temperature T for $CeAuAl_4Ge_2$. (b) $\chi^{-1}(T)$ for $H \parallel c$ and $H \perp c$. Dashed lines are Curie-Weiss fits to the data. (c) $\chi T(T)$ vs T for $H \parallel c$ and $H \perp c$. (d) Magnetization M vs magnetic field H for $H \parallel c$ and $H \perp c$.

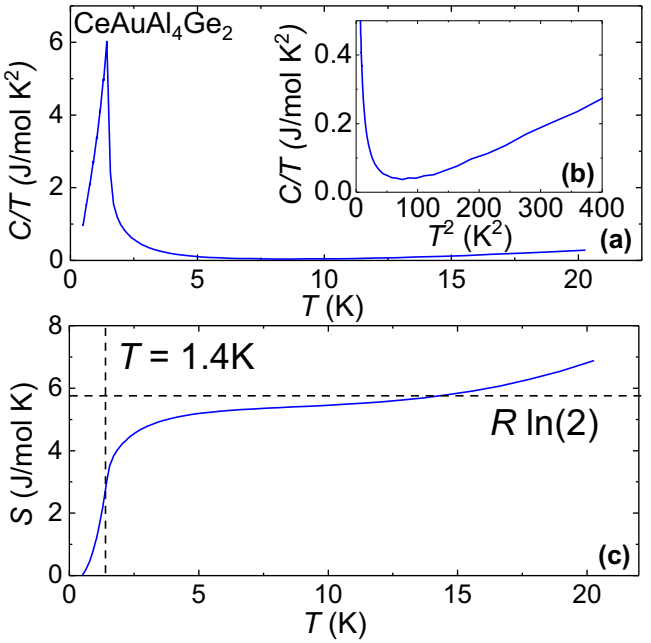

FIG. 3. (a) Heat capacity divided by temperature C/T vs T for $CeAuAl_4Ge_2$. (b) C/T vs T^2. (c) Entropy S vs T. S was calculated as described in the text.

respectively. Thus, the high-temperature Curie-Weiss behavior indicates that although the Ce atoms are arrayed such that their easy axis for magnetization lies in the plane of a geometrically frustrated lattice, they experience a ferromagnetic exchange interaction that would circumvent frustration. With decreasing temperature, a shoulder appears in $\chi^{-1}(T)$ near 25 K for $H \parallel c$ and $H \perp c$, which is likely related to crystal-electric-field splitting of the cerium Hund's rule multiplet. Similar to what is seen in many other Ce-based magnets, this reduces the ground-state magnetic moment and modifies the magnetic exchange interaction [28,29]. This is also evident in the $M(H)$ curves at $T = 1.8$ K for $H \parallel (\perp)\, c$ [Fig. 2(d)], which behave as Brillouin functions and have saturation moments near $M_{sat} \approx 0.4\mu_B$/Ce for $H \parallel c$ and $1.3\mu_B$/Ce for $H \perp c$ above $H \approx 5$ T; these are reduced from the full saturation moment of the $J = 5/2$ cerium multiplet.

The specific heat divided by temperature C/T data are shown in Fig. 3(a), where there is a large λ-like feature associated with the second-order phase transition near $T_M = 1.4$ K. In Fig. 3(b) we show C/T vs T^2, which, for a Fermi liquid, is expected to follow the expression $C/T = \gamma + \beta T^2$ for temperatures well below the Debye temperature θ_D. We find that there is no such region in this data set, possibly because the magnetic fluctuations that precede the ordered state extend up to $T \approx 10$–15 K. Furthermore, the phonon contribution to the heat capacity is only expected to reach the low-temperature T^2 dependence for $T \leqslant \frac{1}{50}\Theta_D$, where Θ_D typically has a value of several hundred kelvins. [30] Although it is not possible to extrapolate C/T vs T^2 to zero temperature to extract a value for γ, we estimate that the value is small ($\gamma \lesssim 15$ mJ/mol K^2). This further suggests that hybridization between the f and the conduction electrons from the Kondo effect is weak. In Fig. 3(c) we show the entropy S vs T obtained by integrating

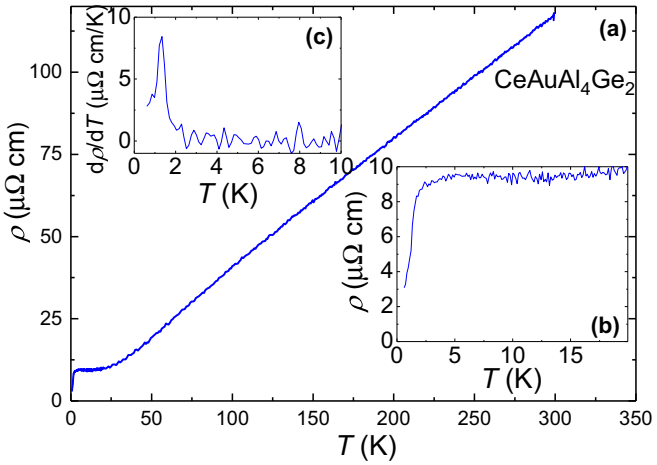

FIG. 4. (a) Electrical resistivity ρ vs temperature T for $CeAuAl_4Ge_2$. (b) Low-temperature region of $\rho(T)$. (c) Derivative of the electrical resistivity with respect to the temperature $\partial\rho/\partial T$ vs T for $H = 0$. The phase transition at $T_M = 1.4$ K appears as a sharp peak.

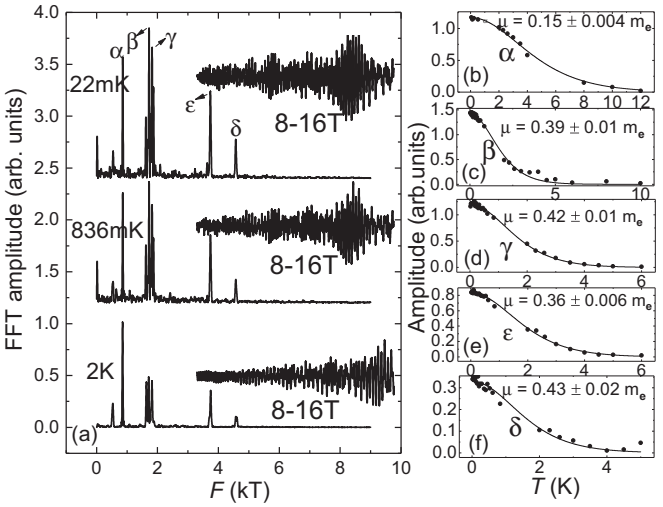

FIG. 5. (a) Quantum oscillations observed in the ac-magnetic susceptibility vs magnetic field H and their fast Fourier transformations plotted vs the frequency. The background was subtracted as described in the text. (b–f) Amplitude vs temperature data fitted with the Lifshitz-Kosvech function.

C/T from 0.5 K. This quantity is only a rough estimate of the $4f$ entropy (recall that the data only reach down to 0.49 K and the electronic contribution could not be isolated from the phonon contribution) but still provides some useful insight. While S increases abruptly at $T_M = 1.4$ K, the entropy only reaches 52% of $R \ln 2$ and recovers 90% of this value near $T = 5$ K. This provides further evidence that magnetic fluctuations persist at temperatures above the ordering temperature.

The electrical resistivity ρ vs T data, where the current was applied in the ab plane, are shown in Fig. 4. Starting from 300 K, $\rho(T)$ decreases monotonically as is expected for a typical metal, where the lattice contribution is the main term. Over the entire temperature range, there is no evidence of Kondo lattice behavior, indicating that $CeAuAl_4Ge_2$ is dissimilar from prototypical heavy fermion materials (e.g., $CeRhIn_5$ [31], $CeCu_2Si_2$ [32], and $CeCu_6$ [33]). Figure 4(b) highlights $\rho(T)$ near the magnetically ordered state, where the curve saturates to a constant value below $T \approx 15$ K, after which it abruptly decreases below $T_M = 1.4$ K due to the removal of spin fluctuation scattering of conduction electrons. The $\frac{\partial\rho}{\partial T}$ vs T data are shown in Fig. 4(c), which clearly shows the transition temperature at 1.4 K in the form of a peak. At low temperatures, $\rho(T)$ saturates towards a value $\rho_0 \approx 1.2\ \mu\Omega$ cm, giving a residual resistivity ratio RRR $= \rho_{300k}/\rho_0 \approx 104$. This large value reveals the high quality of these specimens and is consistent with results from x-ray diffraction. We note that the RRR was determined for several crystals from the same batch, with RRR reaching values as high as 160.

In Fig. 5 we show results from ac-magnetic susceptibility measurements in magnetic fields up to $H = 16$ T with $H \parallel c$ and for 20 mK $< T <$ 2 K. The monotonic background has been removed by subtracting a polynomial curve in order to reveal quantum oscillations, which first appear near 6 T. As evidenced by the small magnetic field required to observe the onset of quantum oscillations, the samples are of very high quality, with an extremely low amount of defect scattering. A fast Fourier transform was performed in order to extract the different frequencies F [Fig. 5(a)]. The Onsager relation $F = A(\Phi_0/2\pi^2)$, where $\Phi_0 = h/2e$ is the magnetic flux quantum, h is the Planck constant, and e is the electron charge, relates the measured frequencies to the extremal cross-sectional areas A of the Fermi surface [34]. For H applied along the c axis, there are several frequencies, which are summarized in Table II. The same frequencies are extracted regardless of the interval of H^{-1} used for the fast Fourier transforms. We focus on the temperature dependence of these frequencies as summarized in Figs. 5(b)–5(f). These data are well described by the expression [35] for a Fermi liquid,

$$A \propto \sqrt{H} R_T R_D,$$

where A is the amplitude of the oscillations, R_D is the damping factor related to the Dingle temperature, and the thermal damping factor $R_T = \frac{\alpha T m^*/H}{\sinh(\alpha T m^*/H)}$. In this expression, m^* is the charge carrier effective mass and $\alpha = 2\pi^2 k_B m_e/e\hbar \approx 14.69$ T/K, where m_e is the free-electron mass. Fits to the data yield small effective masses (Table II), which are comparable to those typically seen in non-$4f$-containing analogs to prototypical heavy fermion materials, e.g., $LaCoIn_5$ [36] and $ThRu_2Si_2$ [37], again indicating that the $4f$ electrons in $CeAuGe_4Al_2$ do not significantly hybridize with the conduction electrons.

IV. DENSITY-FUNCTIONAL THEORY CALCULATIONS

Electronic structure calculations were performed in order to clarify the magnetic ordering and quantum oscillation results. We first investigated the simplest case of ferromagnetic ordering (not shown). Regardless of whether spin-orbit coupling is included, these calculations produce several flat bands near the Fermi level which have a significant f-electron character. These bands result in enhanced effective mass charge carrier quasiparticles, which contradicts the experimental result. Motivated by this disagreement and since our experiments suggest antiferromagnetic ordering, we allowed for antiferromagnetic

TABLE II. Frequency of the orbits (in T) for different pockets in the antiferromagnetic phase. The last two columns list experimental frequencies and masses, on the same row as the nearest matching calculated (calc.) ones.

Orbit	Calc. freq.	Calc. mass (μ_e)	Frequency label	Expt. frequency	Expt. mass (μ_e)
Band a	<20				
Band b, pocket 1	33(0.5)	0.127(0.003)			
Band f, pocket 1	40 (1)	0.17(0.01)			
Band b, pocket 2	76(7)	0.16 (0.02)			
Band b, pocket 3	91(1)	0.21 (0.01)			
Band c, pocket 1	306(2)	0.29 (0.002)			
Band h, pocket 1	782 (2)	0.277 (0.001)			
Band h, pocket 2	833 (2)	0.262 (0.01)			
Band g, pocket 1	626 (2)	0.194(0.002)	1	857	0.15
Band i, pocket 1	1214 (3)	0.395(0.002)	2	1724	0.39
Band i, pocket 2	1304 (4)	0.358 (0.0005)			
Band c, pocket 2	1265(8)	0.6(0.1)			
Band j, pocket 1	1930 (2)	0.652(0.004)	3	1824	0.42
Band j, pocket 2	1967 (3)	0.675 (0.002)			
Band d, pocket 1	2510(40)	0.835(0.005)			
Band k, pocket 1	2445 (5)	0.81 (0.005)			
Band k, pocket 2	2584 (4)	0.75 (0.003)			
Band e, pocket 1	3293 (7)	1.265 (0.005)			
Band e, pocket 2	3680 (5)	1.034 (0.02)			
Band l, pocket 1	3608 (5)	0.79 (0.12)	4	3737	0.36
Band l, pocket 2	3630 (10)	0.715 (0.002)			
Band l, pocket 3	3680 (7)	0.92 (0.002)			
Band f, pocket 2	5000 (5)	1.40(0.2)	5	4570	0.43

alignment by carrying out a density-functional theory calculation using the conventional hexagonal cell instead of the primitive rhombohedral cell. An in-plane antiferromagnetic ordering requires having more than one Ce atom in the ab plane. Hence, the hexagonal cell along the x direction was doubled and the spins were relaxed. In this case an added-on Ce-f Coulomb repulsion (Hubbard) U term has a significant effect on the massive Ce-f character bands near the Fermi level: It moves them away from the Fermi level and this explains the absence of quantum oscillation frequencies with very massive electrons. The features and character of the other bands are largely unaffected by the inclusion of the Hubbard U term. This unit-cell structure has 48 atoms in the unit cell and makes our calculation computationally demanding. For the self-consistent calculation, we used a k-point mesh of $5 \times 11 \times 4$.

In Fig. 6 and Fig. 8, the resulting band structure and Fermi surface of $CeAuAl_4Ge_2$ are presented. Bands corresponding to hole pockets are shown in red, whereas bands corresponding to electron pocket are shown in blue. Without the U term [Fig. 6(a)], there are many flat bands corresponding to Ce-f orbitals close to the Fermi level. When a nonzero U is applied to two electrons on the Ce-f orbital [Fig. 6(b) for $U = 6.80$ eV and Fig. 6(b) for $J = 0.68$ eV], we find that the flat bands move away from the Fermi level by $\approx$4 eV, while the location of other bands is robust even for different values of U. Consistent with the experimental quantum oscillation measurements, which probe only the Fermi surface, in this scenario there is no expectation of flat bands with massive electrons near the Fermi level, suggesting that this is an accurate representation of the band structure. In Fig. 7 we show the projected density of states resulting from this calculation, where the Au, Ge, and Al bands make similar contributions near the Fermi energy.

The calculated Fermi surface (Fig. 8) was subsequently generated using a k-point mesh of $17 \times 35 \times 4$. Because of the doubling of the conventional hexagonal cell only along

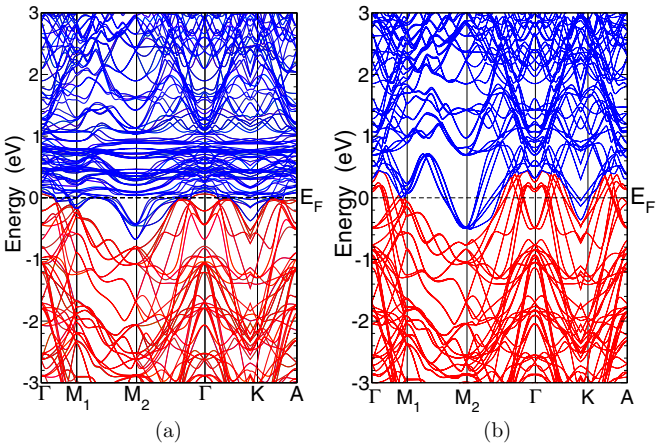

FIG. 6. Band structure in the antiferromagnetic phase of $CeAuAl_4Ge_2$ along the direction Γ-M_1-M_2-Γ-K-A in the rectangular Brillouin zone, where $M_1 = (1/2,0,0)$, $M_2 = (0,1/2,0)$, $K = (2/3, -1/3,0)$, and $A = (0,0,1/2)$. (a) Without U and without spin-orbit coupling. (b) With $U = 6.80$ eV and $J = 0.680$ eV and including spin-orbit coupling.

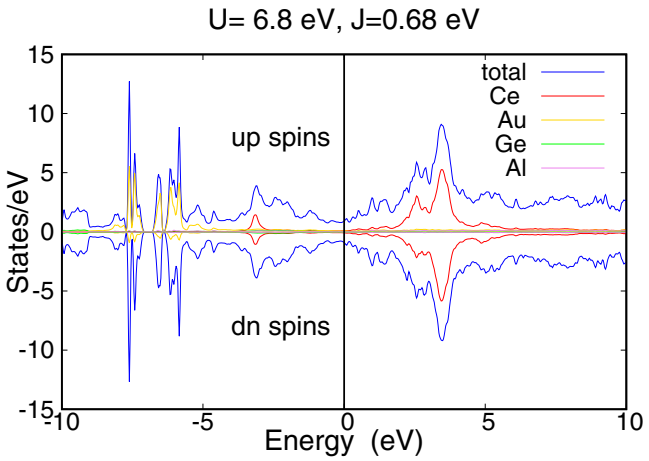

FIG. 7. Projected density of states for $CeAuAl_4Ge_2$, where the antiferromagnetic exchange and on-f-site Coulomb repulsion (Hubbard) U are considered, as described in the text.

the x direction, the two-dimensional Brillouin zone becomes rectangular. The calculated frequencies of the extremal orbits on the Fermi surface for a magnetic field parallel to the c axis (in units of Tesla) along with the band masses are listed in Table II, where they are compared to the five experimentally observed frequencies. While five frequencies were recorded in the experiment, our calculation shows many frequencies. The lowest and highest calculated frequencies are 33 and 5000 T, whereas the experimentally measured ones are 857 and 4500 T, respectively. While there is no one-to-one correspondence between the experimental and the calculated frequencies, we can group the calculated orbits according to size similarity as shown in Table II. When we do that, there is semiquantitative agreement between experiment and calculation. The most significant disagreement is that there are low-frequency orbits (below ∼300 T) and a set of orbits with a frequency around 2500 T that are absent from the experiment. However, the low-frequency orbits, which arise from hole pockets, can be eliminated by pushing the corresponding bands just 4 meV below the Fermi level without affecting the other high frequencies. Since we do not believe that our calculation has this level of accuracy, we find that the only disagreement between our quantum oscillation experiments and our calculations is the absence of the frequency of the order of 2500 T. We also find that the calculated effective masses are in reasonably good agreement with those obtained in experiments.

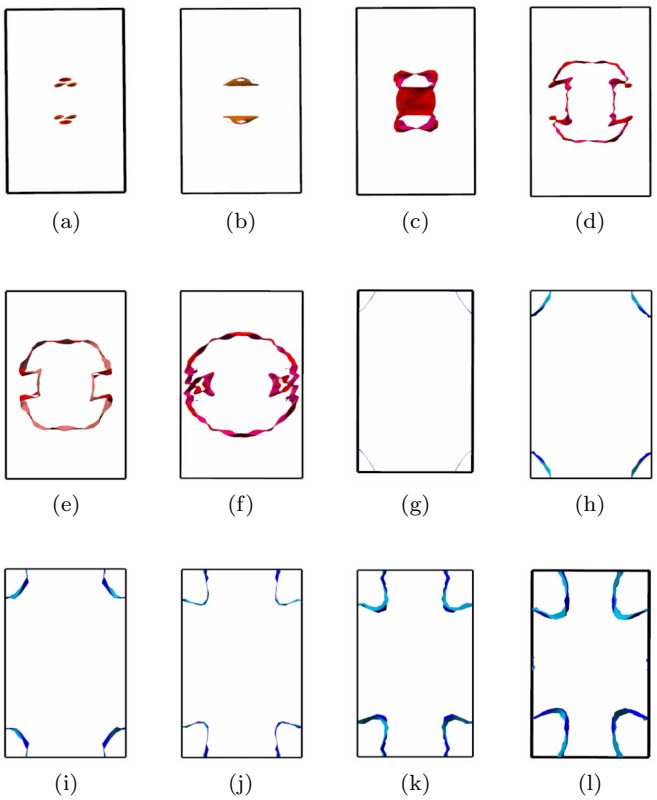

FIG. 8. Fermi surface of $CeAl_4Ge_2Au$ in the antiferromagnetic phase. (a–f) Hole pockets. (g–l) Electron sheets.

V. DISCUSSION AND CONCLUSION

While $CeAuAl_4Ge_2$ does not appear to host strong magnetic frustration, it provides a useful starting point for investigating geometric magnetic frustration in a cerium-based compound without strong Kondo hybridization. This is evidenced by electrical transport and thermodynamic measurements which reveal metallic transport without Kondo coherence, Curie-Weiss behavior (i.e., trivalent cerium), crystal-electric-field splitting that leads to antiferromagnetic exchange at low temperatures, and magnetic ordering with an antiferromagnetic character at $T_M = 1.4$ K. There also appear to be magnetic fluctuations well above T_M, which may indicate weak magnetic frustration. Electronic structure calculations reveal that allowing for the experimentally observed antiferromagnetic order and inclusion of the on f-site Coulomb repulsion (Hubbard) U causes the f-electron bands to move away from the Fermi level, resulting in electronic behavior that is dominated by the s, p, and d bands, which are all characterized by light electron masses. Finally, there is good agreement between the calculated Fermi surface and associated quasiparticle effective masses and the results from measured quantum oscillations in ac-magnetic susceptibility measurements. Besides giving a complete picture of the electronic and magnetic behavior of this compound, this result sets the stage to consider systematically exploring the surrounding chemical phase space, with the aid of electronic structure calculations, in order to seek ways to amplify the low-temperature antiferromagnetic exchange interaction and thereby induce magnetic frustration in what might be a model family of materials.

ACKNOWLEDGMENTS

This work was performed at the National High Magnetic Field Laboratory (NHMFL), which is supported by National Science Foundation Cooperative Agreement No. DMR-1157490, the State of Florida, and the U.S. Department of Energy (DOE). Research by R.B., K.H., Y.L., and D.G. was

supported by the Center for Actinide Science and Technology (CAST), an Energy Frontier Research Center (EFRC) funded by the U.S. DOE, Office of Science, Basic Energy Sciences (BES), under Award No. DE-SC0016568. We acknowledge Stan Tozer for use of his 16-T physical properties measurement system for quantum oscillation measurements of the ac-magnetic susceptibility; he was also partially supported as part of the CAST project.

[1] M. B. Maple, R. E. Baumbach, N. P. Butch, J. J. Hamlin, and M. Janoschek, J. Low Temp. Phys. **161**, 4 (2010).
[2] C. Pfleiderer, Rev. Mod. Phys. **81**, 1551 (2009).
[3] H. v. Lóhneysen, A. Rosch, and M. Vojta, Rev. Mod. Phys. **79**, 1015 (2007).
[4] G. R. Stewart, Rev. Mod. Phys. **73**, 797 (2001).
[5] J. R. Iglesias, C. Lacroix, and B. Coqblin, Phys. Rev. B **56**, 11820 (1997).
[6] S. Doniach, Physica B + C **91**, 231 (1977).
[7] Q. Si, Physica B **378–380**, 23 (2006).
[8] P. Coleman and A. H. Nevidomskyy, J. Low Temp. Phys. **161**, 182 (2010).
[9] M. Vojta, Phys. Rev. B **78**, 125109 (2008).
[10] L. Balents, Nature **464**, 199 (2010).
[11] J. Custers, P. Gegenwart, C. Geibel, F. Steglich, P. Coleman, and S. Paschen, Phys. Rev. Lett. **104**, 186402 (2010).
[12] P. Das, S.-Z. Lin, N. J. Ghimire, K. Huang, F. Ronning, E. D. Bauer, J. D. Thompson, C. D. Batista, G. Ehlers, and M. Janoschek, Phys. Rev. Lett. **113**, 246403 (2014).
[13] K. Sengupta, M. K. Forthaus, H. Kubo, K. Katoh, K. Umeo, T. Takabatake, and M. M. Abd-Elmeguid, Phys. Rev. B **81**, 125129 (2010).
[14] V. Fritsch, N. Bagrets, G. Goll, W. Kittler, M. J. Wolf, K. Grube, C.-L. Huang, and H. v. Löhneysen, Phys. Rev. B **89**, 054416 (2014).
[15] Y. Tokiwa, C. Sting, M.-S. Kim, T. Takabatake, and P. Gegenwart, Sci. Adv. **1**, e1500001 (2015).
[16] W. Selke, Phys. Rep. **170**, 213 (1988).
[17] R. E. Baumbach, H. Chudo, H. Yasuoka, F. Ronning, E. D. Bauer, and J. D. Thompson, Phys. Rev. B **85**, 094422 (2012).
[18] R. E. Baumbach, X. Lu, F. Ronning, J. D. Thompson, and E. D. Bauer, J. Phys.: Condens. Matter **24**, 325601 (2012).
[19] A. P. Ramirez, Annu. Rev. Mater. Sci. **24**, 453 (1994).
[20] Rigaku Oxford Diffraction, CrysAlisPro Software system, version 1.171.37.33 (Rigaku Corp., Oxford, UK, 2016).
[21] P. W, Betteridge, J. R. Carruthers, R. I. Cooper, K. Prout, and D. J. Watkin, J. Appl. Crystal. **36**, 1487 (2003). [We used version 14, build 5911, February 2016.]
[22] L. Palatinus and G. Chapuis, J. Appl. Crystal. **40**, 786 (2007).
[23] X. Wu and M. G. Kanatzidis, J. Solid State Chem. **178**, 3233 (2005).
[24] P. Villars and K. Cenzual, *Pearson's Crystal Data: Crystal Structure Database for Inorganic Compounds, Release 2014/15* (ASM International, Materials Park, OH, 2014).
[25] G. Bergerhoff and I. D. Brown, Inorganic crystal structure database, in *Crystallographic Databases*, edited by F. H. Allen, G. Bergerhoff, and R. Sievers (International Union of Crystallography, Chester, UK, 1987), pp. 77–95.
[26] K. Schwarz, P. Blaha, and G. Madsen, Comp. Phys. Commun. **147**, 71 (2002).
[27] J. P. Perdew, K. Burke, and M. Ernzerhof, Phys. Rev. Lett. **77**, 3865 (1996).
[28] K. W. H. Stevens, *Crystalline Electric Field and Structural Effects in f-Electron Systems*, edited by J. E. Crow, R. P. Guertin, and T. W. Mihalisin (Plenum Press, New York, 1979).
[29] D. A. Joshi, A. K. Nigam, S. K. Dhar, and A. Thamizhavel, J. Magn. Magn. Mater. **322**, 3363 (2010).
[30] A. Tari, *The Specific Heat of Matter at Low Temperatures* (Imperial College Press, London, 2003).
[31] G. Knebel, D. Aoki, J.-P. Brison, and J. Flouquet, J. Phys. Soc. Jpn. **77**, 114704 (2008).
[32] H. Q. Yuan, F. M. Grosche, M. Deppe, C. Geibel, G. Sparn, and F. Steglich, Science **302**, 2104 (2003).
[33] G. R. Stewart, Z. Fisk, J. L. Smith, J. O. Willis, and M. S. Wire, Phys. Rev. B **30**, 1249 (1984).
[34] D. Shoenberg, *Magnetic Oscillations in Metals* (Cambridge University Press, Chester, UK, 1984).
[35] T. Terashima, C. Haworth, H. Takeya, S. Uji, H. Aoki, and K. Kadowaki, Phys. Rev. B **56**, 5120 (1997).
[36] D. Hall, L. Balicas, Z. Fisk, R. G. Goodrich, U. Alver, and J. L. Sarrao, Phys. Rev. B **79**, 033106 (2009).
[37] Y. Matsumoto, Y. Haga, N. Tateiwa, H. Aoki, N. Kimura, and T. D. Matsuda, JPS Conf. Proc. **3**, 011096 (2014).